Shock Waves (1998) 8: 375–381

Shock Waves

Shock wave propagation in a branched duct

O. Igra[1], L. Wang[1], J. Falcovitz[2], W. Heilig[3]

[1] Pearlstone Center for Aeronautical Engineering Studies, Department of Mechanical Engineering, Ben-Gurion University of the Negev, Beer Sheva, Israel
[2] Institute of Mathematics, the Hebrew University, Jerusalem, Israel
[3] Ernst Mach Institute, Eckertstr. 4, D-79104 Freiburg, Germany

Received 15 July 1996 / Accepted 20 February 1997

Abstract. The propagation of a planar shock wave in a 90° branched duct is studied experimentally and numerically. It is shown that the interaction of the transmitted shock wave with the branching segment results in a complex, two-dimensional unsteady flow. Multiple shock wave reflections from the duct's walls cause weakening of transmitted waves and, at late times, an approach to an equilibrium, one-dimensional flow. While at most places along the branched duct walls calculated pressures are lower than that existing behind the original incident shock wave, at the branching segment's right corner, where a head on-collision between the transmitted wave and the corner is experienced, pressures that are significantly higher than those existing behind the original incident shock wave are encountered. The numerically evaluated pressures can be accepted with confidence, due to the very good agreement found between experimental and numerical results with respect to the geometry of the complex wave pattern observed inside the branched duct.

Key words: Shock wave reflection, Shock wave diffraction, Shock wave attenuation

1 Introduction

When a planar shock wave propagates into a uniform cross-section duct, it slowly attenuates due to momentum and energy dissipation via friction and heat transfer. A much faster decay in the shock wave strength is observed when it propagates into a branched duct. In such a case the main mechanism responsible for reducing the shock wave strength is multiple shock wave reflections initiated by the branched duct. Interest in shock wave propagation in branched ducts of various geometries is stimulated by its application in many engineering problems. Some examples are: hazardous explosions in mine shafts; gas transmission pipes; exhaust systems of internal combustion multicylindrical engines and in design of shelters from bomb generated explosions. In most of the above-mentioned examples, one is interested in quickly reducing the intensity (impulse) of the propagating shock, or blast, wave. Studies published in the past three decades were limited to either experimental investigations or approximate theoretical/numerical solutions based on the assumption that the flow is quasi-one dimensional. For example see Dadone et al. (1971), Sloan and Nettleton (1971), Srivastava (1973), Peters and Merzkirch (1975), and Heilig (1975).

Correspondence to: O. Igra
Final editing and publication were unintentionally but unduly delayed, for which the Editor-in-Chief apologizes to the authors.

It is the purpose of the present paper to provide a comprehensive and accurate description of shock wave propagation in a branched duct. The case to be studied is shown in Fig. 1. The experimental part consists of shadowgraphs recording the history of the planar shock wave interaction with, and propagation into, the branched duct shown in Fig. 1. In the theoretical part a two-dimensional numerical solution for the flow field that evolves behind the shock waves transmitted into the branched duct is given.

The experiments were conducted in the 40×110 mm cross-section shock tube of the Ernst Mach Institute in Freiburg, Germany. A 90° branched duct model, shown schematically in Fig. 1, was placed inside the test-section to generate a duct having a rectangular cross-section; 40 mm in view direction and 20 mm in height. A Crantz-Schardin multiple spark camera provided a sequence of shadowgraphs taken during each run with a pre-set time interval. Details regarding the shock tube and the optical system used for the experimental investigation are given in Mazor et al. (1992).

2 Theoretical background

The interaction process of a planar shock wave with a 90° branched duct and its subsequent transmission into the duct's two branches, results in a nonstationary two-dimensional flow. Focusing on the flow which develops

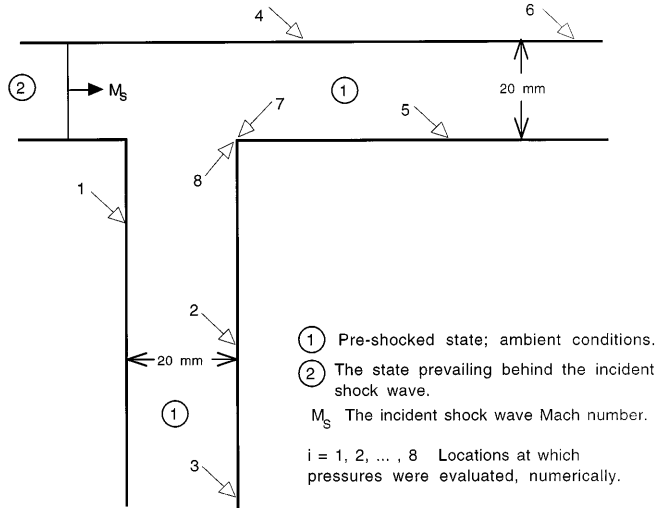

Fig. 1. Schematic description of the investigated flow field

close to the branching segment of the duct (up to 5-6 heights of the duct) one can safely ignore friction and energy (heat transfer) losses. Therefore, the conservation equations of mass momentum and energy, written in vector form, for a two-dimensional, nonstationary, inviscid gas flow are:

$$\frac{\partial}{\partial t}U + \frac{\partial}{\partial x}F(U) + \frac{\partial}{\partial y}G(U) = 0, \tag{1}$$

where,

$$U(x,y,t) = \begin{pmatrix} \rho \\ \rho u \\ \rho v \\ \rho E \end{pmatrix}, \quad F(U) = \begin{pmatrix} \rho u \\ \rho u^2 + p \\ \rho uv \\ (\rho E + p)u \end{pmatrix},$$

$$G(U) = \begin{pmatrix} \rho v \\ \rho uv \\ \rho v^2 + p \\ (\rho E + p)v \end{pmatrix},$$

$$E = e + \frac{1}{2}(u^2 + v^2), \quad p = (\gamma - 1)\rho e.$$

$F(U)$ and $G(U)$ are the flux components in the x- and y-directions, respectively. p, ρ, e, u, v and E are pressure, density, specific internal energy, velocity components and total specific energy, respectively. Equation (1) was solved numerically using the GRP scheme whose principles are given in Ben-Artzi and Falcovitz (1984). In the following only a brief description of this numerical scheme, tailored for the solution of (1) is given. Details regarding this scheme can be found in Igra et al. (1996).

The multi-dimensional GRP method is inherently a formal extension of the one-dimensional GRP scheme. First consider the governing equations for a one-dimensional time-dependent inviscid compressible flow in the (x,t)-plane. These are:

$$\frac{\partial}{\partial t}U + \frac{\partial}{\partial x}F(U) = 0, \tag{2a}$$

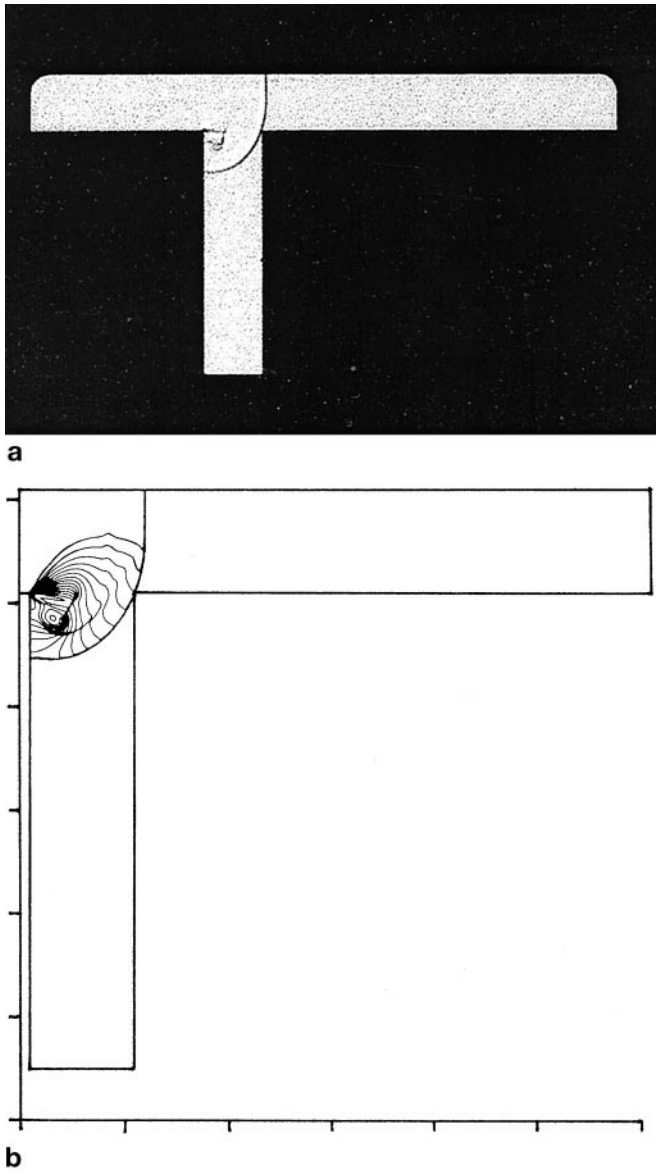

Fig. 2a,b. Wave configuration at t = 28 μs. **a** Experimental results (shadowgraph), and **b** Numerical simulation (isopycnics)

$$U(x,t) = \begin{pmatrix} \rho \\ \rho u \\ \rho E \end{pmatrix}, \quad F(U) = \begin{pmatrix} \rho u \\ \rho u^2 + p \\ (\rho E + p)u \end{pmatrix}. \tag{2b}$$

The flow field is divided into a grid comprising a set of cell-interface points $x_{i+1/2}$, and the i-th cell is the interval $x_{i-1/2} < x < x_{i+1/2}$. The conservative second-order difference scheme for the time integration of the conservation laws, (2a) is:

$$U_i^{n+1} = U_i^n - \frac{\Delta t}{\Delta x_i}[F(U)_{i+1/2}^{n+1/2} - F(U)_{i-1/2}^{n+1/2}], \tag{3}$$

where the time-centered fluxes are obtained by employing the following procedure.

The flow at time level t^n is approximated as piecewise linear in primitive flow variables (velocity, pressure and density) per cell, with discontinuities at cell-interfaces. First, the Riemann problem that correspond to the initial discontinuity (U_L, U_R) extrapolated linearly to cell interfaces is solved, giving rise to the first-order (upwind) fluxes $F(U)^n_{i+1/2}$ and $G(U)^n_{i+1/2}$. This is followed by evaluating the first time- derivatives of flow variables at cell interfaces using analytical expressions that resulted from the GRP analysis. The stage is then set for evaluating the second-order accurate fluxes given by:

$$F(U)^{n+1/2}_{i+1/2} = F(U)^n_{i+1/2} + \frac{\Delta t}{2}\Big[\frac{\partial}{\partial t}F(U)\Big]^n_{i+1/2} \qquad (4)$$

$$\Big[\frac{\partial}{\partial t}F(U)\Big]^n_{i+1/2} = F'(U^n_{i+1/2})\Big[\frac{\partial}{\partial t}U\Big]^n_{i+1/2}$$

Following the integration of the conservation laws, the slope of flow variables in cells are updated, subject to monotonicity constraints designed to avoid erroneous interpolation at cell interface; the Van Leer (1979) monotonicity scheme was imposed on the slopes of primitive variables. Turning now to the two-dimensional flow case, the flow domain is divided into a set of rectangular cells. The finite-volume form of the Euler equations, (1) can be written for each cell as

$$\frac{dU}{dt} = -\frac{1}{A}\sum_{\text{faces}}(F_{n_x} + G_{n_y})\Delta S, \qquad (5)$$

where A is the area of the cell, and $\mathbf{n} = (n_x, n_y)$ and ΔS are the outward unit normal vector and the faces lengths, respectively. Time-centered integration of (5) on each cell (i, j) results in

$$U^{n+1}_{ij} = U^n_{ij} - \frac{\Delta t^n}{A_{ij}}\sum_{\text{faces}}(F^{n+1/2}_{n_x} + G^{n+1/2}_{n_y})\Delta S,$$

where the time-centered normal fluxes $(F^{n+1/2}n_x + G^{n+1/2}n_y)$ at each face are evaluated in a similar way as shown in (4). The main steps are the following. The Generalized Riemann Problem solved at each cell-boundary in order to evaluate the mid-step fluxes as in (4), is the following initial value problem. At x-facing cell-boundaries, (1) is solved with initial data comprising linearly-distributed states on either side, treating the y- momentum conservation law as pure advection. An analogous procedure is performed at y-facing cell-boundaries. The outcome of the GRP analysis is analytic expressions for the primitive variables and their first-order time derivatives at the cell's face. They lead to plug-in expressions for evaluating the fluxes at cell-boundaries according to Eq. (4).

3 Results and discussion

Figures 2a to 5a show shadowgraph photographs taken during an experiment in which the incident shock wave Mach number, before it reached the branching section, is

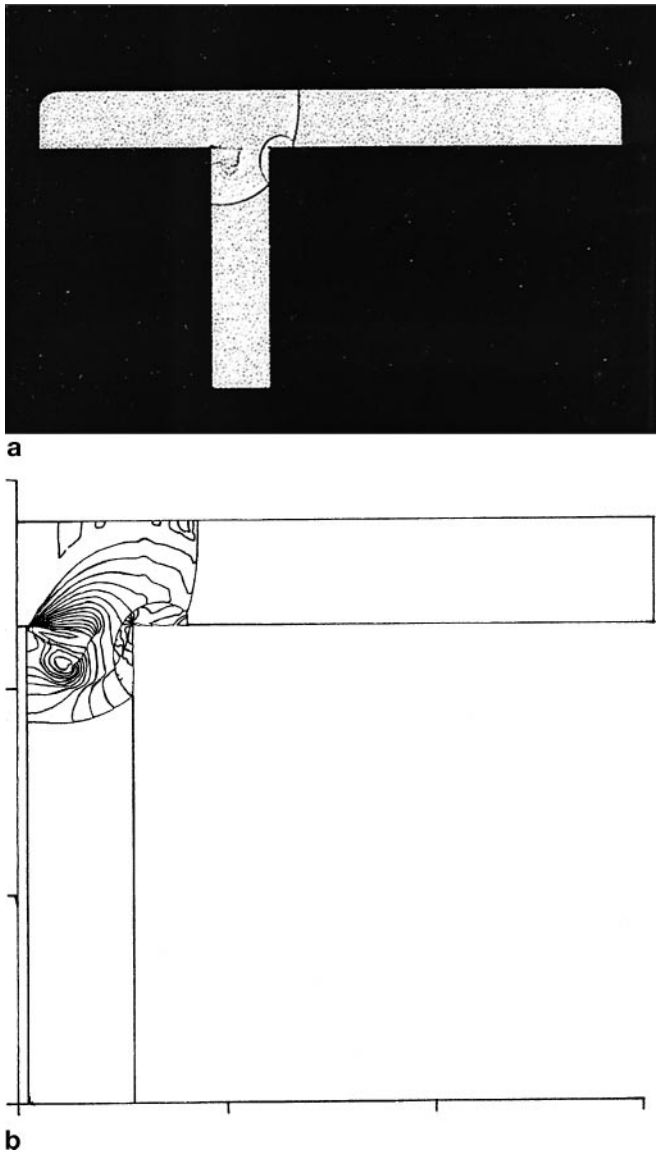

Fig. 3a,b. Wave configuration at t = 40.5 μs. **a** Experimental results (shadowgraph), and **b** Numerical simulation (isopycnics)

M_s= 2.4. The pre-shock pressure and temperature are 1 bar and 15°C, respectively. Figure 3a was taken 12.5 μs after the shadowgraph shown in Fig. 2a, the shadowgraph shown in Fig. 4a was taken 35 μs after that shown in Fig. 3a and the time interval between Fig. 5a and 4a is 75 μs. Numerical simulations made for the above-mentioned times are shown in Figs. 2b to 5b. The lines appearing in these figures are lines of constant density (isopycnics). A comparison between numerical simulations and appropriate shadowgraphs attests to the accuracy of the proposed physical model (1) and its numerical solution. It is apparent that the numerical solution reconstructs the complex wave pattern and its time evolvement very accurately. In Fig. 2 the incident shock wave is seen as it hits the right corner of the branching section. The post-

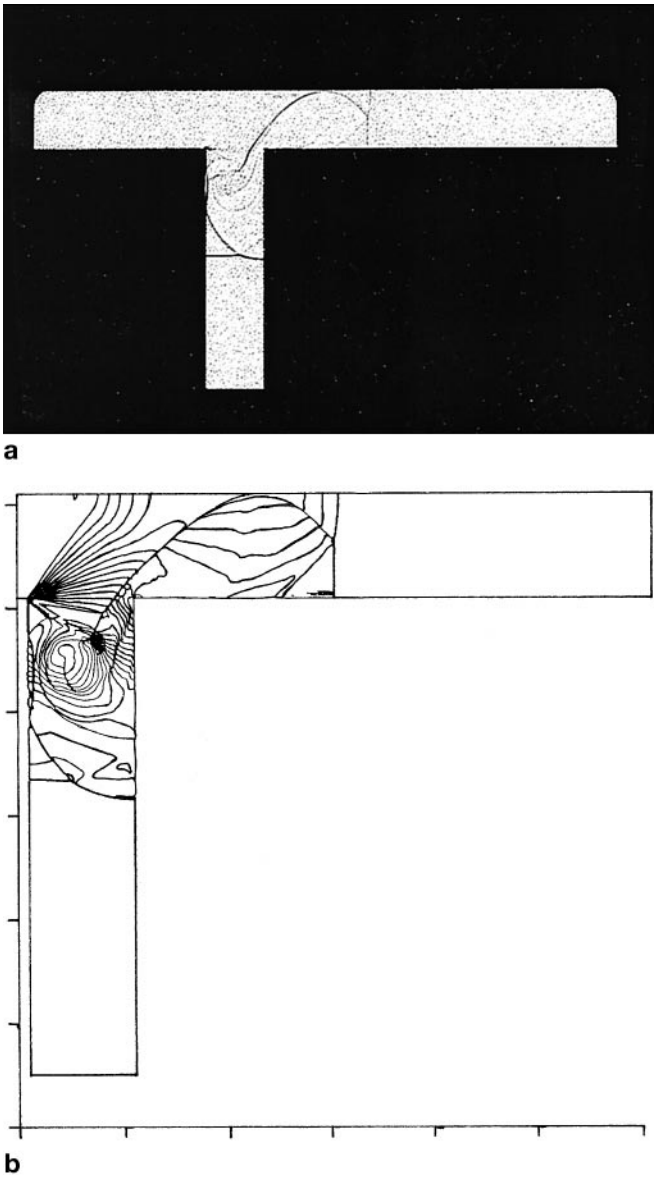

Fig. 4a,b. Wave configuration at t = 75.5 μs. **a** Experimental results (shadowgraph), and **b** Numerical simulation (isopycnics)

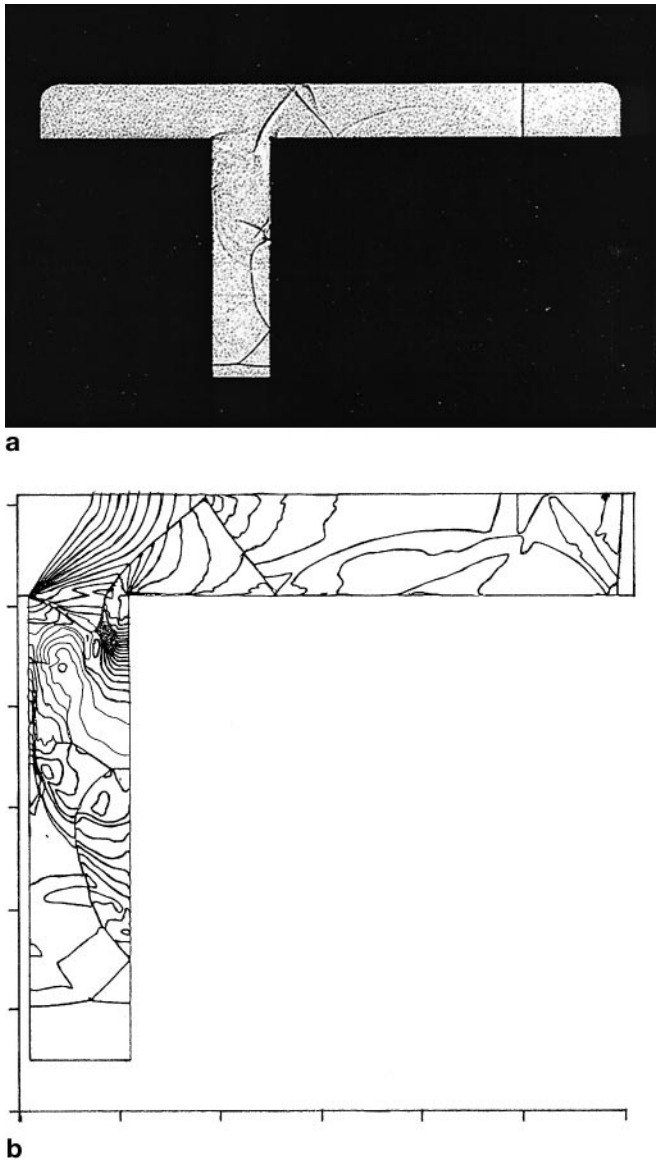

Fig. 5a,b. Wave configuration at t = 150.5 μs. **a** Experimental results (shadowgraph), and **b** Numerical simulation (isopycnics)

shock flow is supersonic. (For $M_s = 2.4$ the post-shock flow Mach number in air is 1.157.) As a result, the flow is deflected into the 90° branch of the duct via a centered rarefaction wave. This centered rarefaction wave is shown very clearly in Fig. 2b (depicting isopycnics); it is hardly noticed on the shadowgraph (Fig. 2a) since the shadowgraph is sensitive to the second density derivatives, which are generally quite small in the fan region away from the corner. However, the center of the rarefaction fan, where strong density gradients prevail, is clearly noticed in both Figs. 2a and 2b. In both figures a secondary shock wave, required for matching the high pressure existing behind the transmitted shock wave and the low post-rarefaction pressure, is observable. The angle of the rarefaction wave head, near the branching segment left corner is about 59° as expected for a flow Mach number of 1.157. 12.5 μs later the incident shock wave has passed the branching section right corner. The transmitted shock wave (in the horizontal part of the branched duct) exhibits a Mach reflection pattern from the duct floor. A regular reflection is evident at the wall of the vertical part of the duct. Both transmitted waves (into the vertical duct and into the horizontal duct) are curved, indicating that the post-shock flows are two-dimensional. In addition to the transmitted and reflected waves, the secondary shock wave mentioned before, is also visible in both Figs. 3a and 3b. Figure 3b provides an exact simulation for the wave pattern shown in Fig. 3a. As time proceeds the transmitted waves prop-

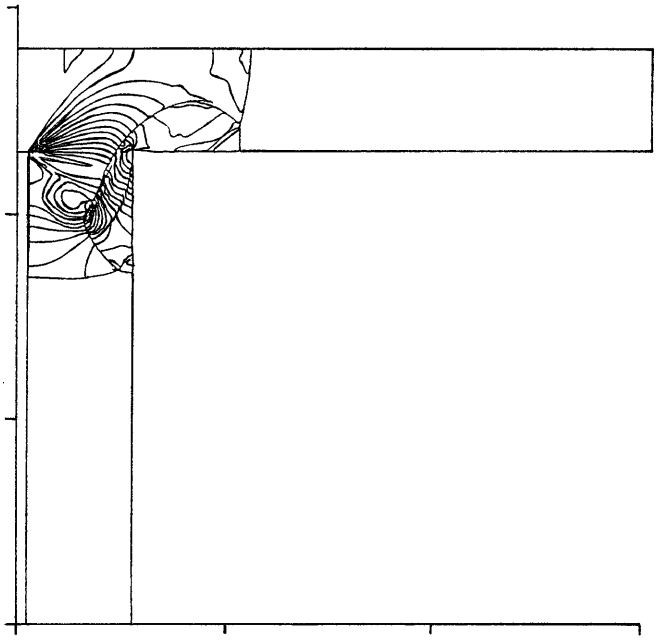

Fig. 6. Numerical simulation of the wave configuration at t = 63 μs

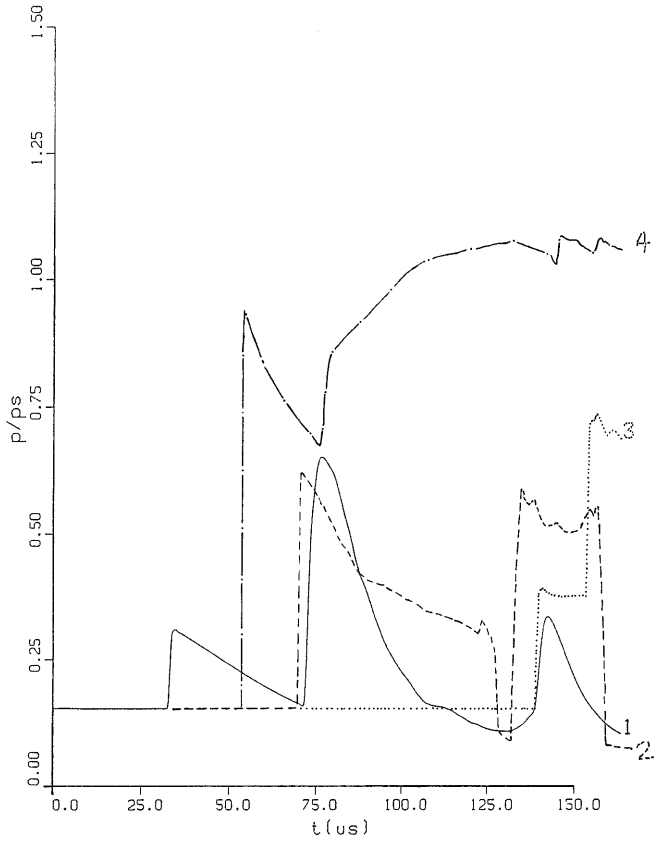

Fig. 7. Calculated pressure history at ports No. 1, 2, 3 and 4

agate further into the two branches of the duct. In Fig. 4, taken 35 μs after Fig. 3, a clear Mach reflection is evident from the walls of both ducts. The shock wave originally reflected from the branching segment right corner is split into two parts. This splitting is a result of its collision with the secondary shock wave. This collision happened 12.5 μs before the event shown in Fig. 4; a record of the collision between these two shock waves is shown in the numerical simulation in Fig. 6. It is clear from this figure that the almost cylindrical, reflected shock wave, shown in Fig. 3, is deformed during its collision with the secondary shock wave (see Fig. 6) and thereafter split into two parts as is evident in Fig. 4. It is also apparent from Fig. 4 that the secondary shock is weakened by its collision with the reflected shock wave (it appears as a brighter and thinner line). In the last shadowgraph, Fig. 5a (taken 75 μs after the one shown in Fig. 4a), the transmitted wave in the horizontal part of the branched duct is almost planar. The weaker shock wave, transmitted through the vertical part of the branching, is still experiencing a Mach reflection. Additional reflections are clearly noticed in both branches of the duct indicating that the flow at this time is still two-dimensional. Again, the numerical simulations (Fig. 5b) reproduces well the complex wave pattern shown in Fig. 5a, indicating the reliability of the proposed physical model (1) and its numerical solution. We may therefore use, with confidence, the proposed numerical solution for assessing pressures which prevail at different locations along the branching duct. The locations where pressure computations were conducted (marked as 1 to 8) are shown in Fig. 1. The calculated pressure histories at these locations are shown subsequently.

The pressure history at ports No. 1 to 4 are shown in Fig. 7. Pressures in this figure, and in the following one, were normalized by the pressure prevailing behind the incident shock wave prior to its interaction with the branching section. It is apparent from Fig. 7 that at port No. 1 the pressure throughout the investigated time will be lower than that existing behind the original incident shock wave. As a matter of fact, the transmitted wave into the 90° branch of the duct is significantly weaker than the original incident shock wave. When it reaches port No. 1 (at about t= 35 μs) its strength is only one third of that of the incident shock wave. It will rise to about 70% of the incident shock wave strength when the reflected shock wave from the branched section right corner hits port No. 1, at about t = 75 μs, and reflects back; see the reflected wave near this position in Fig. 4b. Additional peak is observed at this position, at t $\cong$ 143 μs, when the shock seen over the right branching corner in Fig. 5b passes this station. As observed previously, the pressure in port No. 2 also remains below the value experienced behind the original incident shock wave; see Fig. 7. The transmitted wave reaches this position at about t= 70 μs; it is stronger than the one experienced in port No. 1 since it faces the original flow direction. The second pressure jump at this position, which takes place at t $\cong$ 132 μs, is due to the reflected shock wave which produces a pocket of high pressure over a zone which includes port No. 2; see the wave configura-

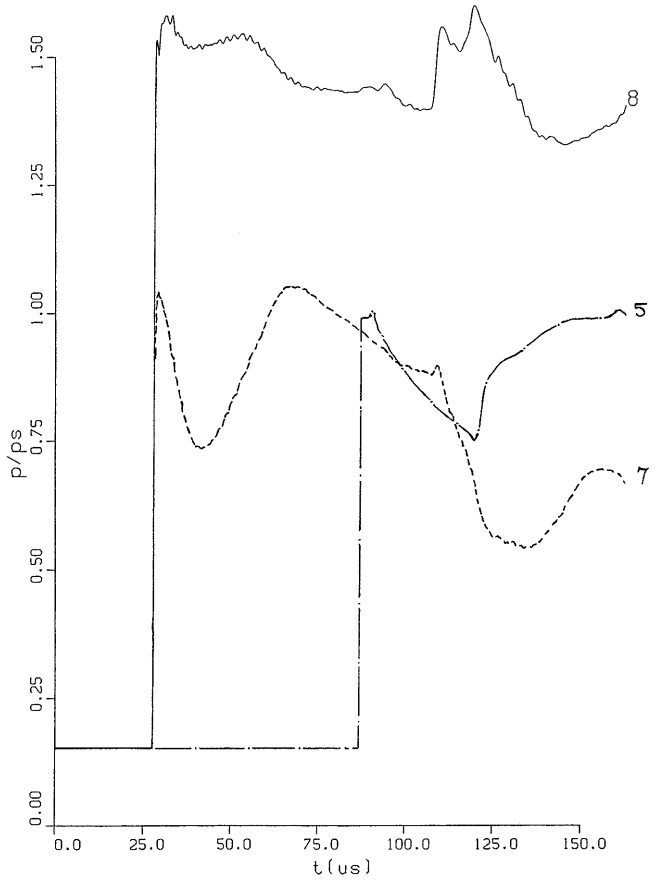

Fig. 8. Calculated pressure history at ports No. 5, 6 and 7

tion in Fig. 5b. This pressure suddenly decreases at t $\cong$ 160 μs, when the Mach stem, which terminates the high pressure pocket (see Fig. 5b), passes port No. 2. The pressure history at port No. 3 is also shown in Fig. 7. The first pressure jump is due to the passage of the transmitted shock wave (its Mach stem, see Fig. 5b), while the second is due to the appearance of the reflected wave. As before, in port No. 3 too, the pressure does not reach the value existing behind the original incident shock wave. Ports 4, 5 and 6 are located along the horizontal part of the branched duct. The transmitted wave in this part is stronger and therefore higher pressures should be expected to prevail at these locations. It is apparent from observing Figs. 7 and 8 that indeed this is the case. The transmitted shock wave reaches port No. 4 at about t = 54 μs and causes the first jump to reach almost 90% of the pressure which prevails behind the original incident shock wave (see Fig. 7). The pressure decreases immediately after this jump due to the influence of the centered rarefaction wave located at the left corner of the branching section (see Fig. 4b). A second pressure rise takes place when the reflected shock wave (shown in Fig. 4b) reaches this port. This is a relatively weak shock (see Fig. 4b) and therefore the pressure jump it causes is relatively small. The pressure continues to rise and exceeds the value that existed behind the original incident shock wave due to compression waves emanated from the duct floor. It can be seen from Fig. 4b that the Mach stem of the transmitted shock wave, in the horizontal part of the branching segment, is stronger than the top part of the reflected shock wave which will hit port No. 4 at t $\cong$ 76 μs. (In the numerical simulations strong shock waves appear as darker lines.) This difference in strength is responsible for the pressure increase during the time interval 78 μs $\leq t \leq$ 145 μs. The pressure history at port No. 5 is shown in Fig. 8. It is similar to that observed for port No. 4 in Fig. 7, with the exception that during the calculated time interval pressures at this port hardly reach the value observed behind the original incident shock wave. The first large pressure jump is associated with the passage of the transmitted shock wave while the second is due to the reflected shock wave from the duct's upper wall. Port No. 6 is placed at the largest distance from the branching section and as a result during the covered computational time (150 μs) all that is observed at this port is the passage of the transmitted shock wave. (It causes a pressure jump of about 95% of that experienced behind the original incident shock wave.) Therefore, the pressure history calculated for port No. 6 is not shown here. The numerical result obtained for the pressure history at port No. 7 is also shown in Fig. 8. The large pressure jump occurring at t $\cong$ 30 μs is due to the passage of the transmitted shock wave (shown in Fig. 2b). It causes a pressure peak slightly higher than the pressure value existing behind the original incident shock wave. This peak quickly decreases due to the presence of the centered rarefaction wave at the branching segment left corner. The appearance of a reflected shock wave near the branching segment right corner (see Fig. 3b) causes the pressure increase shown in Fig. 8 for 40 μs $\leq t \leq$ 69 μs. At later times, this reflected wave is weakened due to its interaction with the centered rarefaction wave, placed at the branching segment left corner, it causes a decrease in pressure with increasing time. It should be noted that in port No. 7 (as well as in ports Nos. 4 and 5) pressures are mostly below the value existing behind the original incident shock wave. Only temporarily does it slightly exceed this value. This is not the case with the pressure history observed at port No. 8, which is also shown in Fig. 8. At this location the pressure significantly exceeds the value which exists behind the original incident shock wave. Throughout the investigated time it is at least 38% higher; frequently it is 50% higher than the pressure prevailing behind the original incident shock wave. This should not be surprising since port No. 8 experiences almost a head-on collision with the transmitted shock wave. At no other ports does such an event take place.

From the foregoing discussion it is apparent that the flow which evolves behind the transmitted waves is truly nonstationary and two-dimensional. Approximating it as quasi-one-dimensional, as done in the past, will lead to significant errors, especially in proximity to the branching section. The shock wave transmitted down the 90° branch is weaker than the one propagating along the original direction. Therefore, if one looks for protection from the high pressure generated behind the incident shock wave,

the best place to be is in the 90° branching tunnel, preferably near its left wall. The worst place will be in proximity to the branching segment right corner.

4 Conclusions

The proposed physical model for describing planar shock wave interaction and propagation in 90° branching duct, and its numerical solution are capable of describing accurately the considered phenomenon. The excellent agreement between the wave pattern shown on shadowgraph records and the appropriate numerical simulations attest to this statement. It should be noted here that an agreement between wave geometries in shadowgraphs and in their numerical simulations is not always a guarantee for a perfect agreement between the real flow and its numerical simulations. For confirming a complete agreement it is advisable to compare, in addition to the wave geometry, some of the flow properties. Such a comparison was made in a recent study of Igra et al. (1996), in which the GRP numerical results were compared with shadowgraphs and with measurements of peak post shock pressures. The very good agreement that was reported there (Igra et al. 1996) for a similar flow provides the necessary additional support for the present claim for excellent agreement between experimental findings and numerical simulations. Of course, the proposed model and its numerical solution can easily be applied to other branching geometries (angles). The flow developed in the branching duct is unsteady and two-dimensional. While locally pressures higher than those which prevail behind the incident shock wave can be found downstream of the branching segment, over most of the duct surface (downstream of the branching segment) the prevailing pressures are lower than those existing behind the original incident shock wave. This indicates the efficiency of branching in attenuating the incident shock wave. In proximity to the branching segment both transmitted shock waves are not planar. They experience mostly a Mach reflection. Only further downstream of the branching section, in both branches of the duct, these shock waves approach a planar shape. At this stage both shocks are much weaker than the original incident shock wave and the flow approaches a one-dimensional pattern.

References

Ben-Artzi M, Falcovitz J (1984) A second-order Godunov-type scheme for compressible fluid dynamics. J Comp Phys 55:1

Dadone A, Pandolfi M, Tamanini F (1971) Shock waves propagating in a straight duct with a side branch. In: Stollery JL, Gaydon AG, Owen PR (eds:) Shock Tube Research. Chapman and Hall, London, 17/1-17/13

Dekker BEL, Male DH (1967/8) Fluid dynamic aspects of unsteady flow in branched ducts. Proc Instn Mech Engrs 182:167

Heilig WH (1975) Propagation of shock waves in various branched ducts. In: Kamimoto G (ed:) Modern Developments in Shock Tube Research. Shock Tube Research Society, Japan:273-283

Igra O, Falcovitz J, Reichenbach H, Heilig W (1996) Experimental and numerical study of the interaction between a planar shock wave and a square cavity. J Fluid Mech 313:105

Mazor G, Igra O, Ben-Dor G, Mond M, Reichenbach H (1992) Head-on collision of normal shock waves with a rubber-supported wall. Phil Trans R Soc Lond A 338:237

Peters F, Merzkirch W (1975) ZAMM 55T, 1467

Sloan SA, Nettelton MA (1971) The propagation of weak shock waves through junctions. In: Stollery JL, Gaydon AG, Owen PR (eds:) Shock Tube Research. Chapman and Hall, London, 18/1-18/14

Srivastava JP (1973) Israel J Tech 11:223

Van Leer B (1979) Towards the ultimate conservative difference scheme. J Comp Phys 32:101